ELSEVIER

Thermochimica Acta 384 (2002) 71–83

thermochimica acta

www.elsevier.com/locate/tca

# Thermal expansion of TATB-based explosives from 300 to 566 K

Jon L. Maienschein*, F. Garcia

*Energetic Materials Center, Lawrence Livermore National Laboratory, P.O. Box 808, L-282, Livermore, CA 94550, USA*

**Abstract**

We report thermal expansion measurements and coefficient of thermal expansion (CTE) for LX-17-1 (92.5 wt.% 1,3,5-triamino-2,4,6-trinitrobenzene (TATB), 7.5 wt.% Kel-F 800) from 300 to 558 K. Samples uniaxially-compressed at 300 K show an axial CTE of $(2.7 + 0.42T) \times 10^{-6}$ K$^{-1}$ and a radial CTE of $(48 + 0.16T) \times 10^{-6}$ K$^{-1}$; the different axial and radial CTE indicate a small degree of alignment of the TATB molecules under uniaxial compression. LX-17-1 that was pressed in a die heated to 375 K showed additional growth in the 350–400 K temperature range during heating; apparently residual strain is produced in the heated Kel-F during pressing and is released when the material is reheated and the Kel-F softens. We observed irreversible ''ratchet'' growth from temperature cycling, and also found that LX-17-1 continues to expand when held at 524–558 K for periods of 4–5 h. Self-heating during thermal soak at 546–566 K indicated exothermic thermal decomposition.


*Keywords:* TMA; Thermal expansion; Decomposition; Explosives; TATB

## 1. Introduction

Thermal expansion of energetic materials is an important parameter in the overall response of these materials to high temperature environments such as a fire. For example, when exposed to high temperatures, the expansion of the energetic material may lead to such diverse actions as partial or complete filling of void space, extrusion into areas not initially containing energetic materials or even out of the system, or pressurization of containment with increased reaction rates or possible rupture of the containment. The eventual thermal reactions may be quite different for the preceding options, and therefore thermal expansion of energetic materials must be understood and quantified to support work to predict thermal reaction and explosion behavior of energetic materials.

Kolb and Rizzo measured the thermal expansion of 1,3,5-triamino-2,4,6-trinitrobenzene (TATB) crystals over the temperature range of 214–377 K [1]. Stull and Ashcroft measured the coefficient of thermal expansion (CTE) of LX-17-1 (92.5 wt.% wet-aminated TATB, 7.5 wt.% Kel-F 800 binder) over the range of 223–343 K [2]. Finally, the LLNL Explosives Handbook reports without attribution CTE values for LX-17 for two temperature ranges (219–288 and 288–347 K) and a CTE value for PBX-9502 (95 wt.% dry-aminated TATB, 5 wt.% Kel-F 800 binder) at 200 K [3]. Unfortunately, none of these studies extended measurements to high temperatures that are of current interest in studies of the safety of energetic materials. Dallman and Wackerle reports that expansion measurement were made by Cady for PBX-9502 and LX-17 from 220 to 533 K; however, no data are given except for total volume expansion of 10% between 293 and 525 K [4].

In the work reported here, we measured the thermal expansion of LX-17-1 from 300 to 558 K for samples

* Corresponding author. Tel.: +1-925-423-1816; fax: +1-925-422-2382.
*E-mail address*: maienschein1@llnl.gov (J.L. Maienschein).

0040-6031/02/$ – see front matter 
PII: S0040-6031(01)00778-X

uniaxially-pressed from molding powder; parts were pressed both at room temperature and in a die heated to 375 K. We measured both radial and axial expansion during heating and also during prolonged holding at the final temperature. We measured sample mass losses resulting from the high temperature. We calculated the radial and axial CTE as a function of temperature, measured growth of LX-17-1 held at 524–558 K, and observed self-heating from thermal decomposition at 546–566 K.

## 2. Experimental

### 2.1. LX-17-1 sample preparation

We used LX-17-1 molding powder (LLNL lot B915) for this work; the designation LX-17-1 refers to LX-17 made with wet-aminated TATB. Pellets of LX-17-1 were uniaxially-pressed in a conventional double-acting compaction die without mold release, using a single pressing cycle of 5 min at 200 MPa. We pressed most pellets at room temperature, and obtained a density of $\approx$1.88 g cm$^{-3}$ (96.7% theoretical maximum density, TMD). A few were pressed in a die that was preheated to 375 K before the LX-17-1 was loaded, with no subsequent heating; the die cooled by several degrees during the loading and pressing operations. These pellets had a slightly higher density of $\approx$1.89 g cm$^{-3}$ (97.4% TMD). Two sizes of pellets were used, as shown in Table 1, to give a wide range of the length/diameter (*L*/*D*) ratio.

### 2.2. Thermal expansion apparatus

We made thermal expansion measurements with a DuPont 941 thermal mechanical analyzer (TMA) which was controlled by a DuPont 990 thermal analyzer. The data were collected from the 990 thermal analyzer by a Hewlett-Packard 3497A data logger, and stored and analyzed with a Macintosh computer using Igor software. As shown in Fig. 1, the TMA held the sample vertically in a quartz tube located inside a furnace; a thermocouple was located next to the sample and a quartz motion probe sat on top of the sample. The growth of the sample as it is heated by the

Table 1
Static dimensional and mass data for LX-17-1 samples that were ramped to a final temperature and immediately cooled[a]

| Sample ID | Sample *L*/*D* | Pressing temperature (K) | Initial length (mm) | Initial diameter (mm) | Final length (mm) | Final diameter (mm) | Volume change (%) | Mass change (%) | Density change (%) |
|---|---|---|---|---|---|---|---|---|---|
| Axial ramp to 523 K | | | | | | | | | |
| 1 | 1.9 | 293 | 8.4836 | 4.3800 | 8.5598 | 4.4196 | + 2.7 | −0.50 | −3.14 |
| 3 | 1.9 | 293 | 8.5217 | 4.3740 | 8.6182 | 4.4120 | + 2.9 | −0.12 | −2.94 |
| 5 | 0.33 | 293 | 2.9515 | 8.6792 | 2.9972 | 8.7630 | + 3.5 | −0.09 | −3.49 |
| 8 | 1.9 | 373 | 8.4811 | 4.3637 | 8.5954 | 4.4018 | + 3.1 | −0.17 | −3.19 |
| 9 | 0.33 | 373 | 2.9286 | 8.6462 | 2.9591 | 8.7173 | + 2.7 | −0.15 | −2.79 |
| 10 | 1.9 | 373 | 8.4176 | 4.3561 | 8.5623 | 4.4018 | + 3.9 | −0.17 | −3.88 |
| 13 | 0.33 | 373 | 2.9083 | 8.6360 | 2.9743 | 8.7300 | + 4.5 | −0.19 | −4.49 |
| Axial ramp at 553 K | | | | | | | | | |
| 26 | 1.9 | 293 | 8.4023 | 4.3764 | 8.5192 | 4.4094 | + 2.9 | −0.25 | −3.09 |
| Radial ramp at 523 K | | | | | | | | | |
| 2 | 1.9 | 293 | 8.5573 | 4.3739 | 8.6563 | 4.4069 | + 2.7 | −0.21 | −2.82 |
| 4 | 1.9 | 293 | 8.5300 | 4.3800 | 8.6233 | 4.4196 | + 2.9 | −0.08 | −2.93 |
| 6 | 0.33 | 293 | 2.9464 | 8.6700 | 2.9845 | 8.7605 | + 3.4 | −0.09 | −3.39 |
| 7 | 0.33 | 293 | 2.9210 | 8.6716 | 2.9540 | 8.7401 | + 2.7 | −0.09 | −2.75 |
| 11 | 0.33 | 373 | 2.9083 | 8.6385 | 2.9566 | 8.7224 | + 3.6 | −0.16 | −3.66 |
| 12 | 1.9 | 373 | 8.4988 | 4.3510 | 8.6436 | 4.4018 | + 4.1 | −0.21 | −4.13 |
| Radial ramp at 555 K | | | | | | | | | |
| 27 | 1.9 | 293 | 8.3591 | 4.3764 | 8.5039 | 4.4145 | + 3.5 | −0.21 | −3.60 |

[a] Pellets with *L*/*D* of 1.9 had mass of 0.2495 ± 0.0017 g; pellets with *L*/*D* of 0.33 had mass of 0.3224 ± 0.0014 g. Final dimensions were measured after sample had cooled to room temperature.

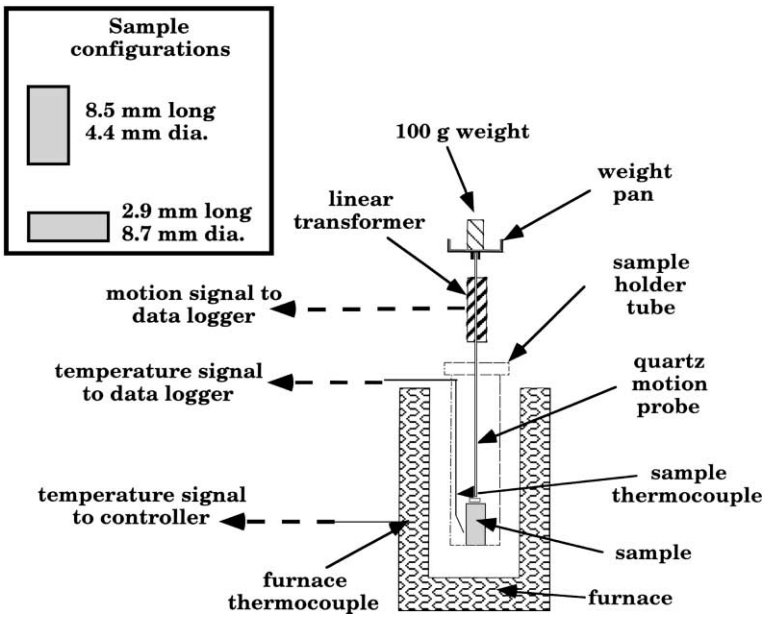


Fig. 1. Schematic diagram of DuPont 941 thermal mechanical analyzer, not to scale. Also shown are sample configurations.

furnace was measured by a linear transformer that converted the vertical motion of the quartz motion probe to a voltage that was recorded by the data logger.

The sample was heated at a constant rate, 5 K $min^{-1}$, as measured by the thermocouple located adjacent to the sample; consistent positioning of this thermocouple run-to-run was required for reproducible results. A faster heating rate would have been preferable in that each thermal cycle would have been of shorter duration, and the instrument drift would have probably been less. However, a faster rate would have led to a significant temperature gradient within the sample, whereas for a rate of 5 K $min^{-1}$ we calculated a temperature gradient of less than 1 K, based on thermal conductivity data [3] and heat transfer formulae [5]. We held a few samples at the final temperature for periods up to 4 h to observe their behavior.

We measured thermal expansion of both sample sizes in the axial (i.e. along the axis of the cylinder) and radial (i.e. along the cross-section of the cylinder) directions. For axial measurements, the cylinder was set on end in the quartz sample holder with the quartz motion probe resting on the other end, while for radial measurements the cylinder was set on its side and the quartz motion probe rested on the upper curved surface of the cylinder (the end of the quartz motion probe was about 5 mm wide, so it did not slip off of the curved surface).

We used NIST thermal expansion standards (copper and stainless steel) to determine the TMA calibration constant, and to check the proper operation of the apparatus. We used In, Sn, and Pb to calibrate the temperature against their melting points.

Pycnometric measurements of the total solid or skeletal volume of each sample were made using a Quantachrome MPY-1 Micropycnometer and helium gas. The pycnometer was calibrated with steel balls provided by the manufacturer, and was accurate to about $\pm 0.004$ $cm^3$.

### 2.3. Calibration of TMA

From measurements with NIST standards (copper and stainless steel), we determined that the TMA calibration ‘‘constant’’ had a 3% standard deviation; therefore, the length data are accurate to $\pm 3\%$ of their values. There was a small but consistent change in the calibration ‘‘constant’’ between low and high sample temperatures; this was presumably due to drift in the response of the linear transformer as the instrument

was warmed by heat from the furnace. However, this effect was sufficiently small compared to the overall accuracy that we did not attempt further temperature stabilization of the instrument, and we used a fixed value of the calibration "constant". This drift did become more significant, however, when we held samples at 520–560 K for up to 4 h, partly as a result of the lower overall change of the sample dimensions during this time. We measured this drift using quartz standards from NIST and corrected growth measurements at constant high temperatures accordingly.

From melting points of pure In, Sn and Pb, the temperature data were consistently low by ≈3 °C between 430 and 600 K; this offset had essentially no effect on the CTE measurement, since CTE is calculated from temperature differences.

We checked the thermal stability of the TMA controller and TMA furnace during thermal soak with a quartz sample in the TMA. The TMA furnace used for expansion measurements during thermal soak gave an upward temperature drift of 1–2 K over the 4 h soak period, with ±0.5 K noise in the temperature signal. We switched to another TMA furnace for three thermal soak runs with no expansion measurements; with this furnace the sample temperature was isothermal within the noise of ±0.2 K.

## 3. Results

### 3.1. Measurements with LX-17-1

In addition to the dynamic TMA growth data, we measured the static dimensions and mass of the sample before and after each run. The static data for each run are shown in Table 1 for samples which were ramped to a set temperature and immediately cooled, and in Table 2 for samples which were ramped to a set temperature and held there for about 4 h before cooling. In addition to the measured data, Tables 1 and 2 also show the calculated volume increase, mass loss, and density decrease during each experiment. Three samples are shown in Table 2 as "static data only". These were tested using only the TMA furnace and sample holder, which were physically removed from the housing that held the quartz motion probe and linear transformer. We thought the samples might ignite and damage the motion probe and linear

Table 2
Static dimensional and mass data for LX-17-1 samples that were ramped to a final temperature and held at that temperature for about 4 h before cooling[a]

| Sample ID | Initial length (mm) | Initial diameter (mm) | Final length (mm) | Final diameter (mm) | Volume change (%) | Mass change (%) | Density change (%) | Notes |
|---|---|---|---|---|---|---|---|---|
| Axial ramp/soak at 524–529 K | | | | | | | | |
| 14 | 8.4430 | 4.3764 | 8.5900 | 4.4380 | +4.6 | −0.75 | −5.14 | 4.0 h at 524 K |
| 22 | 8.4176 | 4.3764 | 8.5242 | 4.4094 | +2.8 | −0.75 | −3.46 | 4.3 h at 529 K |
| Axial ramp/soak at 534 K | | | | | | | | |
| 15 | 8.4201 | 4.3764 | 8.5980 | 4.4380 | +5.0 | −1.30 | −6.00 | 3.9 h at 534 K |
| Axial ramp/soak at 555 K | | | | | | | | |
| 19 | 8.4125 | 4.3764 | 8.4709 | 4.3917 | +1.4 | −5.80 | −7.10 | 4.5 h at 555 K |
| Radial ramp/soak at 526 K | | | | | | | | |
| 21 | 8.4176 | 4.3764 | 8.5293 | 4.4120 | +3.0 | −0.88 | −3.75 | 4.2 h at 526 K |
| 23 | 8.4277 | 4.3764 | 8.5369 | 4.4094 | +2.8 | −0.71 | −3.44 | 4.2 h at 526 K |
| Radial ramp/soak at 558 K | | | | | | | | |
| 20 | 8.4582 | 4.3764 | 8.5293 | 4.3942 | +1.7 | −5.38 | −6.93 | 4.1 h at 558 K |
| Static data only—no dynamic dimensional measurements | | | | | | | | |
| 16 | 8.4353 | 4.3764 | 8.5547 | 4.4120 | +3.1 | −2.80 | −5.69 | 4.0 h at 546 K |
| 17 | 8.4658 | 4.3790 | 8.5395 | 4.3942 | +1.6 | −6.00 | −7.45 | 3.9 h at 558 K |
| 18 | 8.3896 | 4.3764 | 8.2550 | 4.3307 | −3.6 | −16.2 | −13.1 | 4.8 h at 566 K |

[a] All samples had a *L*/*D* ratio of 1.9 and were pressed at 293 K; sample masses were 0.2338 ± 0.0007 g. Final dimensions were measured after sample had cooled to room temperature.

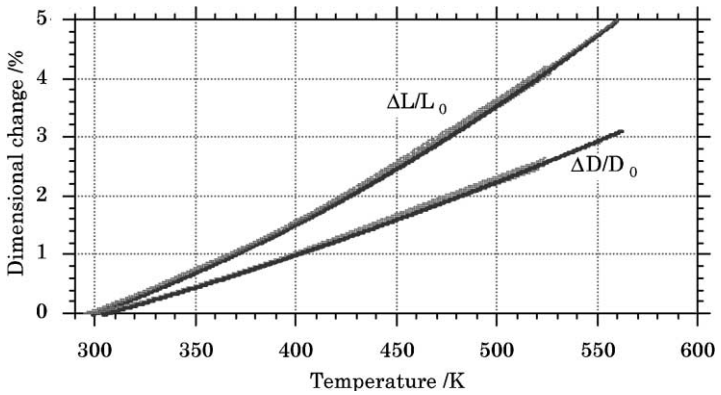


Fig. 2. Dimensional growth data for LX-17-1 heated at 5 K $min^{-1}$. Data are shown for all runs in Tables 1 and 2, except for axial growth measurements using thin samples (samples 5, 9, 13), measurements with samples pressed at 373 K (samples 8–13), and runs where no dynamic data were recorded (samples 16–18). Data were recorded with a temperature resolution of 0.15 K, and are shown as dotted lines. In addition, second-order polynomials fit to each set of data are shown.

transformer when exposed to higher temperatures, and so we made one such run each at 546, 558, and 566 K to verify that ignition would not occur.

The expansion data from the TMA are shown in Fig. 2 as percent change in length and in diameter, referenced to the initial dimensions. In addition, second-order polynomials fit to the complete data set for axial growth and for radial growth are shown, to show that this gives a good fit to the data. As discussed below, the data for samples that were pressed at 373 K are not included in Fig. 2. Also, the data for axial growth of samples with *L*/*D* of 0.33 are not included; these samples were so thin that the growth data were noisy and inconsistent.

Averaged expansion data for samples 8 and 10, which were pressed at 373 K, are shown in Fig. 3. Also shown are averaged data for samples 1 and 3, which were pressed at room temperature. The hot-pressed samples expanded more slowly at low temperatures, but then expanded at a greater rate for temperatures above 350 K; the maximum effect is seen at 385 K. At still higher temperatures, the rate of expansion of hot-pressed pellets approaches that of the samples pressed at room temperature.

Expansion data for samples that were held for about 4 h at elevated temperature are shown in Fig. 4. At 524–529 K there is little expansion during the hold period. At higher temperatures, the samples shrink as a result of the loss of material through sublimation and decomposition.

We observed yellow residue condensed on the upper cool portions of the TMA sample holder above the furnace for samples run above 523 K, which we ascribed to TATB sublimation [6,7]. The quantities were greater at higher temperatures and for samples held for long times at high temperatures. For the run held for 4.8 h at 566 K, we were able to collect 2.2 mg of condensed material and estimated that the total was 4–6 mg. Based on this measurement and the observed amount of condensed material in other runs, we estimate that about 1 mg condensed during the 3.9 h run at 558 K, and less than 0.5 mg collected during the

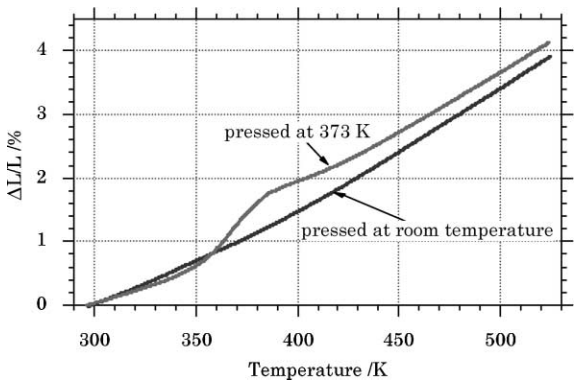


Fig. 3. Dimensional growth data for LX-17-1 heated at 5 K $min^{-1}$, comparing growth of samples pressed at 373 K to growth of samples pressed at room temperature. Data are shown for samples 1, 3, 8, and 10 in Table 1.

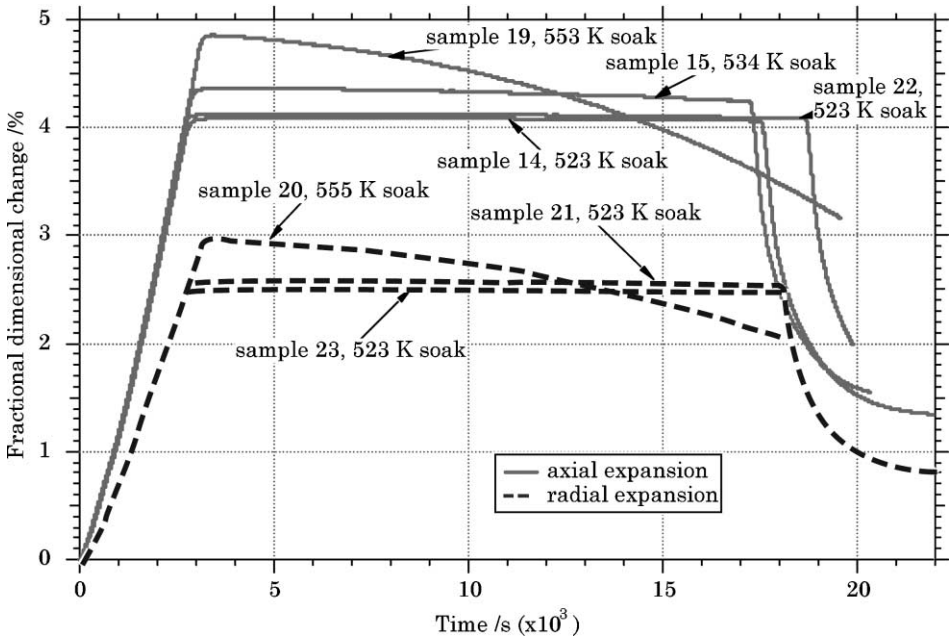


Fig. 4. Expansion data for samples that were held at temperature for several hours.

4 h run at 546 K. The condensed material was darker at the highest temperatures, indicating partial decomposition.

Pycnometric measurements were made on all samples shown in Table 2, along with four unheated pellets. For all heated samples except sample 18, the skeletal volumes ranged from 0.116 to 0.121 $cm^3$, indistinguishable from the skeletal volumes of four unheated pellets which ranged from 0.119 to 0.121 $cm^3$. Sample 18, held at 566 K for 4.8 h, had a skeletal volume of 0.106 $cm^3$, showing significant decomposition and sublimation loss of TATB at this high temperature.

## 4. Discussion

### 4.1. Coefficient of thermal expansion

The CTE of a material is defined as the fractional change in length per unit change in temperature, and is given in units of per Kelvin. At a given temperature, the fractional change in length is defined by the ratio of length change to the length at that temperature. The data shown in Fig. 2 were recorded based on the initial length of the sample, $L_0$. To calculate the CTE, we first converted the length and diameter data shown in Fig. 2 to be based on the length or diameter at temperature, as follows:

$$\frac{\Delta L}{L} = \frac{\Delta L/L_0}{1 + (\Delta L/L_0)} \tag{1}$$

We then fit a second-order polynomial in temperature (K) to the converted $\Delta L/L$ (%) and $\Delta D/D$ (%) data; the polynomials (with standard deviations for each coefficient) were

$$\frac{\Delta L}{L} = -1.95 \pm 0.01 + 2.74 \pm 0.69 \times 10^{-4} T + 2.10 \pm 0.01 \times 10^{-5} T^2 \tag{2}$$

$$\frac{\Delta D}{D} = -2.21 \pm 0.01 + 4.84 \pm 0.06 \times 10^{-3} T + 8.03 \pm 0.07 \times 10^{-6} T^2 \tag{3}$$

The polynomial fits to the data were quite good, as shown by the low standard deviation in the coefficients. To calculate the CTE, we divided Eqs. (2) and (3) by 100 to convert from percentage to fractional

growth, and differentiated with respect to temperature

$$\mathrm{CTE_{axial}} = (2.7 + 0.42T) \times 10^{-6}\,\mathrm{K^{-1}} \quad (4)$$

$$\mathrm{CTE_{radial}} = (48.0 + 0.16T) \times 10^{-6}\,\mathrm{K^{-1}} \quad (5)$$

For these small expansions, the volumetric CTE can be calculated as

$$\mathrm{CTE_{volumetric}} = \mathrm{CTE_{axial}} + 2\mathrm{CTE_{radial}} \quad (6)$$

or

$$\mathrm{CTE_{volumetric}} = (99 + 0.74T) \times 10^{-6}\,\mathrm{K^{-1}} \quad (7)$$

Clearly the form of the calculated CTE will depend on how we fit the $\Delta L/L$ and $\Delta D/D$ data. We see from Fig. 2 that the data slope upward for $\Delta L/L$ and less strongly for $\Delta D/D$. This indicates increasing growth at increasing temperatures, so the CTEs are increasing as well. We could have represented the high temperature portion of the radial expansion data with a straight line, but chose to be consistent between the two sets of data. The second-order polynomial fits the data as well or better than alternative functions, and is simple; therefore, we chose to represent the data in this form.

We see from Fig. 2 and Eqs. (4) and (5) that the axial growth is greater than the radial growth of these samples, and also is more strongly temperature-dependent. The thermal expansion of crystalline TATB along the *c*-axis (perpendicular to the aromatic ring) is 10–30 times greater than along the *a*- and *b*-axes (in the plane of the aromatic ring) [1], so the enhanced axial expansion of LX-17 indicates partial orientation of the TATB crystals during pressing, with the aromatic ring being forced perpendicular to the axis along which compaction pressure is applied. The ratio $\mathrm{CTE_{axial}/CTE_{radial}}$ ranges from 1.4 to 1.7 over our temperature range, only 5% of the difference in CTEs along the TATB axes, so the extent of alignment is rather small.The CTE results in Eqs. (4), (5) and (7) are shown in Fig. 5 along with the available literature data. Our results are somewhat higher than for most literature values, although our volumetric measurements are reasonably consistent with those of Kolb and Rizzo [1]. However, the literature measurements are for significantly lower temperatures than in our work. To compare with Cady's measurement of 10% volume expansion from 293 to 525 K [4], we determine from Fig. 2 a linear expansion of 4.15% and diametral expansion of 2.6% at 525 K. These together give a volumetric expansion of 9.6%, in excellent agreement with Cady's work.

### 4.2. Hot-pressed versus cold-pressed samples

As seen in Fig. 3, the expansion behavior of hot-pressed LX-17-1 is significantly different than that of LX-17-1 pressed at room temperature (cold-pressed).

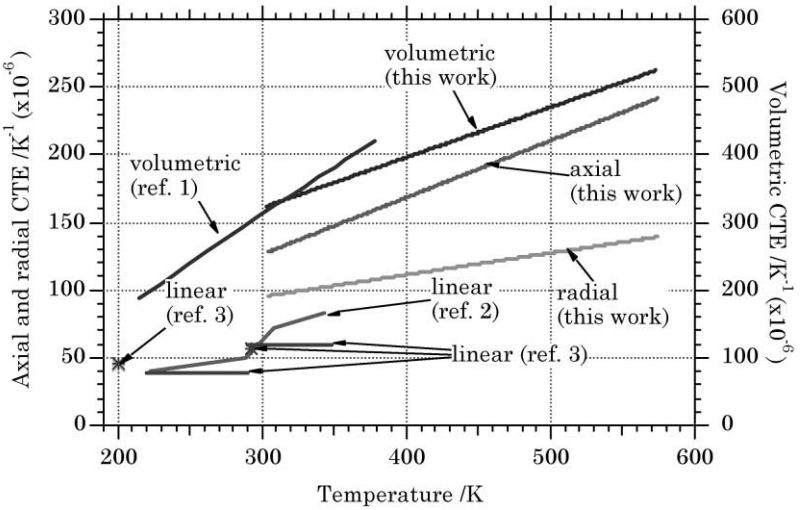


Fig. 5. Coefficient of thermal expansion data for cold-pressed LX-17-1 from this work (axial, radial, and volumetric), compared with literature values (axial and linear) for LX-17-1 and for TATB.

Apparently pressing with a die initially at 373 K results in additional residual strain in the pellet, perhaps because the Kel-F is much softer at the higher pressing temperature; this strain is relieved when the Kel-F softens as the pellet is heated above 350 K. This transition temperature is well above the glass-transition temperature of Kel-F, which ranges from 303 to 307 K with increasing amounts of a solid filler [8,9]. However, it is consistent with multiple melting peaks seen by differential scanning calorimetry at about 340 and 370 K [9,10]. By averaging expansion data from two axial growth samples with $L/D = 1.9$ (samples 8 and 10) and comparing the resultant slope with that from cold-pressed samples, we calculate the ratio of axial CTEs for hot-pressed and cold-pressed samples as a function of temperature; a similar calculation is done for radial growth samples 11 and 12. The results, shown in Fig. 6, indicate that the hot-pressed samples grow slightly more slowly at low and high temperatures, but grow much more rapidly in the 350–400 K temperature range. Overall, hot-pressed samples show more expansion than cold-pressed samples. We have not tested hot isostatically-pressed LX-17-1 samples, but expect that they would behave similarly to the hot uniaxially-pressed samples.

### 4.3. Dimensional and mass changes after thermal cycling

From the data in Table 1, we see that irreversible growth occurred in the LX-17-1 when it was thermally cycled. This is the known "ratchet growth" effect with TATB/Kel-F energetic materials [11]. When heated to 523 K and then cooled, the sample volumes increased $3.3 \pm 0.6\%$. The hot-pressed samples appeared to expand slightly more, $3.7 \pm 0.7\%$, than the cold-pressed samples, $3.0 \pm 0.3\%$, although the difference is not statistically significant. There was also a slight mass loss (about 0.5 mg), due to sublimation as shown below of $0.17 \pm 0.11\%$; this was the same for hot- and cold-pressed samples. The large standard deviation in mass loss is the result of the high value for sample 1—without this sample the mass loss was $0.14 \pm 0.05\%$. The increase in volume and mass loss led to decreases in sample density, $3.4 \pm 0.6\%$ for all samples. The hot-pressed samples showed a larger decrease, $3.7\pm$

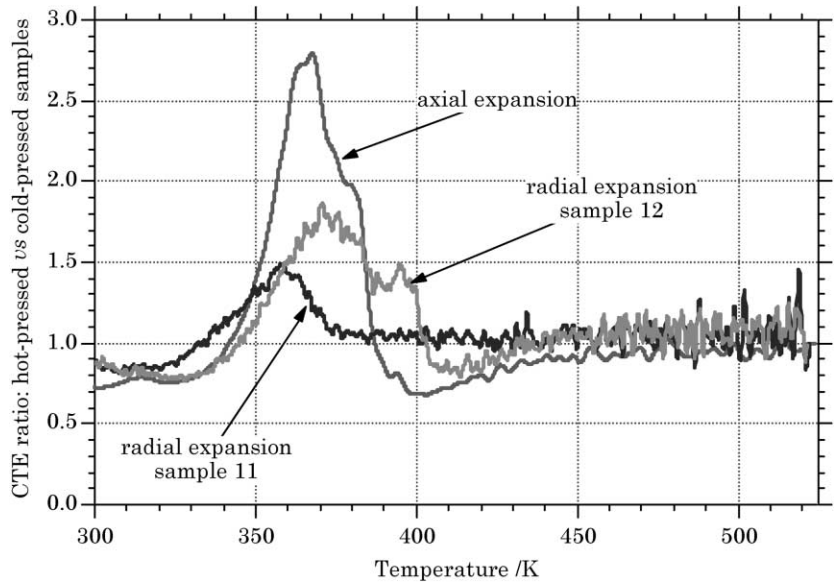


Fig. 6. Comparison of CTE values for samples pressed at 373 K with those pressed at room temperature. CTE ratios are given for axial expansion (samples 8 and 10 compared with samples 1 and 3), and for radial expansion (samples 11 and 12 compared with samples 2 and 4). Samples 8 and 10 were consistent and are shown as one curve. Samples 11 and 12 were not consistent, so each is shown separately.

0.6%, than the cold-pressed samples, $3.1 \pm 0.3\%$, although again the difference is not statistically significant. Two samples thermally cycled to 553–555 K gave results essentially the same as at 523 K. Volume increases were 2.9 and 3.5%, mass losses were 0.25 and 0.21%, and density decreases were 3.1 and 3.6%.

The standard deviations for volumetric increase, mass loss, and density decrease, when normalized by the respective mean values, are 18, 36, and 16% of the respective means. In as much as these static measurement were done before and after each run using a calibrated calipers and a calibrated balance, we think that the most of the error is due to the heterogeneous nature of the LX-17 material. We note that the change in density is largely due to the increase in volume, since the decrease in mass is very low, and therefore the relatively high standard deviation of the mass loss (35% of the mean) does not significantly increase the error in the density decrease.

### 4.4. Dimensional and mass changes during thermal soak

In Fig. 4, we see that samples held at 534 K and above for prolonged periods became shorter during the thermal soak, as a result of mass loss from sublimation and decomposition. Although not as clear from Fig. 4, the samples (all cold-pressed) held at 523–529 K also lost mass during the thermal soak. The mass loss (1.8–2.1 mg) from these four samples was $0.78 \pm 0.07\%$, significantly higher than the mass loss from the thermal ramp alone. The increase in volume, $2.9 \pm 0.1\%$, was about the same as for samples with the thermal ramp alone, but the density decrease, $3.6 \pm 0.2\%$, was higher because of the higher mass loss.

During the thermal soak competing mechanisms are active—sublimation and decomposition leading to shrinkage by removal of material, and decomposition leading to formation of gas bubbles inside the material and resulting expansion. In order to consider growth of confined LX-17-1 (e.g. confined by a container), we need to determine the relative contributions of sublimation and decomposition to the observed thermal soak behavior, and calculate the growth of LX-17-1 during thermal soaks in the absence of sublimation or loss of decomposition products.

### 4.5. Correcting thermal soak growth data to eliminate mass losses

To distinguish between sublimation and decomposition mass losses, we calculated the mass loss rate for each sample during the thermal soak period, based on the surface area of the pellet during the soak period. We assumed that all of the mass loss occurred during the thermal soak; this should be reasonable, since most of the mass loss at 523 K occurred during the thermal soak. Both side and end surface areas were used in the calculation. The results are tabulated in Table 3, and shown in Arrhenius form in Fig. 7, where we see two different slopes. The lower temperature slope, from

Table 3
Calculated mass loss rates for samples held in thermal soak, assuming essentially all mass loss was during thermal soak[a]

| Sample ID | Soak temperature (K) | Soak time (h) | Calculated hot length (mm) | Calculated hot diameter (mm) | Mass change (g) | Mass loss rate (g mm$^{-2}$ s$^{-1}$) |
|---|---|---|---|---|---|---|
| 14 | 524 | 4.0 | 8.4448 | 4.3770 | −0.0018 | 8.5E−10 |
| 21 | 526 | 4.2 | 8.4194 | 4.3770 | −0.0021 | 9.5E−10 |
| 23 | 526 | 4.2 | 8.4296 | 4.3770 | −0.0017 | 7.7E−10 |
| 22 | 529 | 4.3 | 8.4195 | 4.3770 | −0.0018 | 8.0E−10 |
| 15 | 534 | 3.9 | 8.4220 | 4.3770 | −0.0031 | 1.5E−09 |
| 16 | 546 | 4.0 | 8.4373 | 4.3770 | −0.0067 | 3.2E−09 |
| 19 | 555 | 4.5 | 8.4145 | 4.3770 | −0.0138 | 5.8E−09 |
| 17 | 558 | 3.9 | 8.4678 | 4.3796 | −0.0144 | 7.0E−09 |
| 20 | 558 | 4.1 | 8.4602 | 4.3770 | −0.0129 | 6.0E−09 |
| 18 | 566 | 4.8 | 8.3916 | 4.3770 | −0.0386 | 1.5E−08 |

[a] Dimensions while hot were calculated from initial dimensions in Table 2 and from axial and radial CTE formulae, Eqs. (4) and (5). Dimensional changes during thermal soak were sufficiently small that their effect on the pellet surface area could be neglected. Mass changes are from data in Table 2.

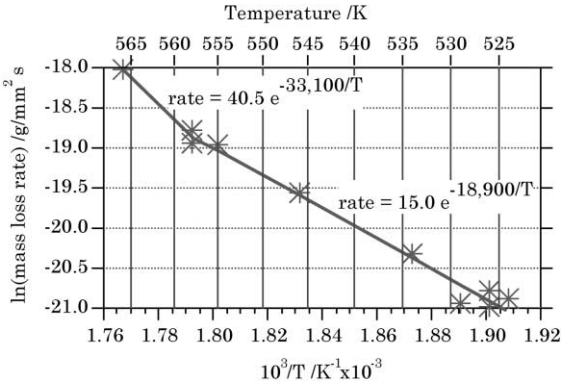


Fig. 7. Mass loss rate as a function of temperature during thermal soak, showing slope break at 555–558 K. Lower temperature mass loss is sublimation or endothermic decomposition, higher temperature mass loss is exothermic decomposition.

524 to 558 K, presumably represents mass loss from sublimation or mass loss from the initial endothermic decomposition of TATB. The activation energy for the lower temperature region, $160 \pm 8$ kJ mol$^{-1}$, is reasonably consistent with the activation energy for TATB sublimation of 177 kJ mol$^{-1}$ estimated from Garza's sublimation data at 423–473 K [6], and with McGuire and Tarver's estimated activation energy of the initial decomposition step of 176 kJ mol$^{-1}$ [12]. The slope at higher temperatures, 558–566 K, presumably represents mass losses from decomposition. The activation energy at higher temperature, $275\pm$ 44 kJ mol$^{-1}$, is consistent with McGuire and Tarver's estimate of 250 kJ mol$^{-1}$ for the second, exothermic, decomposition step [12].

The shrinking of the samples shown in Fig. 4 is primarily the result of the sublimation or initial endothermic decomposition of TATB (Kel-F 800, a copolymer of chlorotrifluorethylene and vinylidine fluoride, is thermally stable like many fluorinated polymers and is not expected to decompose at these temperatures). As mentioned above, we observed the deposition of a yellow residue on the cool regions of the TMA, which we ascribe to TATB sublimation. The initial mass loss of TATB from decomposition results in the elimination of water [12], so this would not give a volatile yellow residue. We therefore conclude that sublimation is occurring in the samples; some low temperature decomposition may be occurring as well. With the mass loss rates shown in Table 3 and Fig. 7, we can correct the growth data in Fig. 4 for the effect of mass losses. The resulting growth curve should represent the growth behavior of confined or massive LX-17-1 where sublimation is restricted and products are confined.

To correct for mass loss, we assume that mass is lost over all the surface area at equal rates. First considering the length measurements (i.e. axial expansion measurement), the mass lost from the ends is

$$\text{mass lost} = 2A\left(\frac{\mathrm{d}m}{\mathrm{d}t}\right)\Delta t \tag{8}$$

where $A$ is the surface area of one end (in mm$^2$), $\mathrm{d}m/\mathrm{d}t$ the mass loss rate (plus value indicates mass loss) (in g mm$^{-2}$ s$^{-1}$), and $\Delta t$ is the duration over which sublimation occurred.

Dividing the mass lost by the density gives the volumetric loss, and dividing by the surface area $A$ gives the length change that results from the mass loss at the ends

$$L_{\text{corr}} = L_{\text{meas}} + 2.0\left(\frac{\mathrm{d}m}{\mathrm{d}t}\right)\frac{\Delta t}{\rho} \tag{9}$$

where $L_{\text{corr}}$ is the corrected length (in mm), $L_{\text{meas}}$ the measured length of sample (in mm), and $\rho$ is the sample density (in g mm$^{-3}$).

Therefore, we correct the measured length by adding $2.0(\mathrm{d}m/\mathrm{d}t)\Delta t/\rho$ to each length value during the soak, with $\Delta t = 0$ at the beginning of the soak period.

Similarly, to correct the diameter of a sample (i.e. radial measurement), we write the mass lost from the sides as

$$\text{mass lost} = A'\left(\frac{\mathrm{d}m}{\mathrm{d}t}\right)\Delta t \tag{10}$$

where $A'$ is the surface area of side of sample (in mm$^2$).

Again, dividing mass lost by the density gives the volumetric loss, and dividing by the surface area of the side, $A'$, gives the radial change that results from the mass loss on the side. In terms of diameter

$$D_{\text{corr}} = D_{\text{meas}} + 2.0\left(\frac{\mathrm{d}m}{\mathrm{d}t}\right)\frac{\Delta t}{\rho} \tag{11}$$

where $D_{\text{corr}}$ is the corrected diameter (in mm), and $D_{\text{meas}}$ the measured diameter (in mm).

Therefore, we correct the measured diameter by adding $2.0(\mathrm{d}m/\mathrm{d}t)\Delta t/\rho$ to each diameter value during the soak, with $\Delta t = 0$ at the beginning of the soak period.

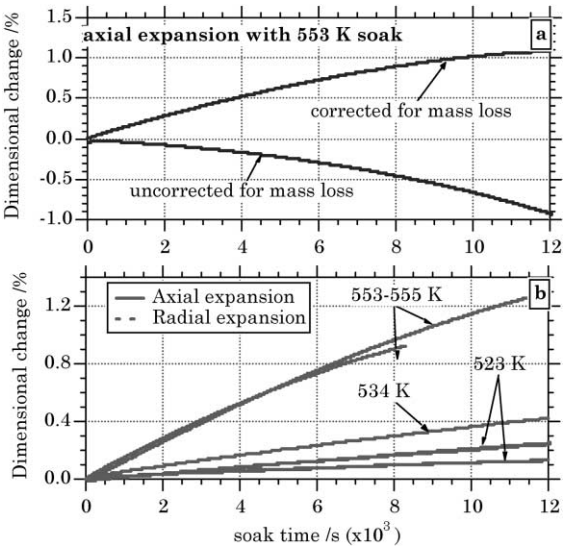


Fig. 8. (a) Radial expansion data for thermal soak at 553 K, uncorrected and corrected for sublimation losses, showing magnitude of correction. (b) Expansion data during thermal soak for several runs, corrected for sublimation losses.

### 4.6. Corrected thermal soak expansion results

Thermal expansion data during the thermal soak, corrected using Eqs. (9) and (11), are shown in Fig. 8 for the samples shown in uncorrected form in Fig. 4. In addition, the uncorrected and corrected data are shown for one sample, to illustrate the magnitude of the correction. The mass loss rates, d*m*/d*t*, used in the correction are given in Table 3, and the density was calculated from the initial density and the thermal expansion to the soak temperature. All samples show continued expansion during the thermal soak, with the axial and radial expansions being essentially equal. As expected, we see greater expansion at higher temperatures. The cause for the continued expansion during the thermal soak is not known, but our speculation is that low levels of decomposition are occurring, generating decomposition gaseous products inside the solid which form bubbles and expand the LX-17-1. Since the gas is retained within the sample, there is no mass loss from decomposition (except for that small fraction that occurs near the surface). Presumably the bubbles break and release their contents, with resultant loss of mass from the sample, when a greater amount of decomposition occurs.

Regardless of the mechanism, the data in Fig. 8 can be used to estimate the continued expansion of LX-17-1 under thermal soak conditions. There is considerable uncertainty in the absolute growth, given the large correction that we made for sublimation losses. Because of this uncertainty, we choose to characterize the growth during thermal soak by the approximate slope of the growth over the region of most constant growth rate. The axial growth rate at 523 K is low, about $(1–2) \times 10^{-5}\%\ s^{-1}$. The axial growth at 534 K is about $3 \times 10^{-5}\%\ s^{-1}$. At 553–555 K, the growth rate is about $20 \times 10^{-5}\%\ s^{-1}$.

With growth during soak ascribed to gas bubble formation the volumetric growth rate is equal to the rate of porosity formation in the LX-17-1. We can approximate the volumetric growth rate as the sum of the linear growth rate and two times the diametral growth rate. We therefore estimate the volumetric growth rate to be $5 \times 10^{-5}\%\ s^{-1}$ at 523 K, $9 \times 10^{-5}\%\ s^{-1}$ at 534 K, and $60 \times 10^{-5}\%\ s^{-1}$ at 553–555 K. The density of the material is presumably decreasing at the same rate.

### 4.7. Porosity measured in sample soaked at 566 K

As described above, we saw a significant difference from the starting material in pycnometer measurements only for sample 18, which was held at 566 K for 4.6 h (without dynamic expansion measurement). The measured skeletal volume of 0.106 $cm^3$, and the measured bulk volume of 0.122 $cm^3$ indicate pore volume of 0.016 $cm^3$, or 13% porosity in this sample. This is consistent with the density decrease of 13% shown in Table 2 for this sample.

### 4.8. Self-heating during thermal soak

As exothermic decomposition occurs in an energetic material, the material may increase in temperature if the heat release is faster than heat loss. We were able to observe this during thermal soak for the three samples run with the stable furnace (samples 16–18 in Table 2). The extent of self-heating ranged from 1.8 to 3.0 K, as shown in Fig. 9. Also shown in Fig. 9 are four runs with quartz samples, to show the stability of the furnace in the absence of self-heating. The temporal behavior of the temperature drift can, in each case, be divided into two regions of essentially linear behavior, as shown in Fig. 9. It was beyond the scope of this

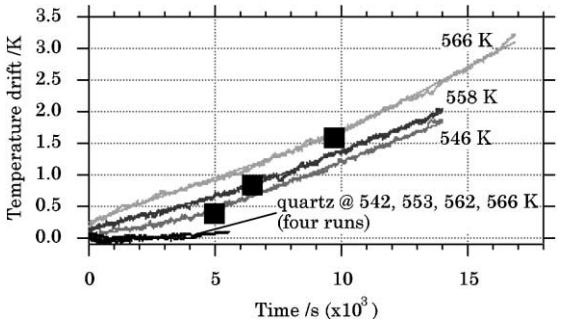


Fig. 9. Self-heating of three LX-17-1 samples during thermal soak. Temperature drift data for four runs with quartz samples show the stability of the TMA thermal system. The straight lines are fit to the data, with the square on each data set indicating the separation point for the linear regions. The rates of temperature increase for each temperature are: 7.3 and $15 \times 10^{-5}$ K $s^{-1}$ at 546 K, 11 and $15 \times 10^{-5}$ K $s^{-1}$ at 558 K, and 14 and $21 \times 10^{-5}$ K $s^{-1}$ at 566 K.

work, but the heat release behavior can be related to decomposition kinetics, if the heat of decomposition is known. Our observation of steady temperature increase indicates that initial endothermic decomposition reactions in TATB decomposition [12] involve small amounts of heat compared to the subsequent exothermic steps, so that the exothermic heat release overwhelms the heat absorbed in the endothermic steps.

## 5. Summary

We report thermal expansion measurements of LX-17-1 from 300 to 558 K, and calculate linear and volumetric CTE. The LX-17-1 samples used here were uniaxially compacted, and showed axial expansion 1.4–1.7 times greater than radial expansion, indicating a small degree of alignment of the TATB molecules under uniaxial compression. LX-17-1 that was hot-pressed showed additional growth in the 350–430 K temperature range, presumably the release of extra strain in the hot-pressed material as the Kel-F softens. We observed irreversible ''ratchet'' growth in samples cycled to 520–558 K. During thermal soak at 524–558 K, samples became smaller due to loss of material from sublimation; however, when corrected for the sublimation losses, we found that the LX-17-1 continued to grow during a thermal soak, albeit at a low rate. At 555–558 K, thermal decomposition became significant, leading to additional sample shrinkage beyond that due to sublimation. LX-17-1 held at 566 K for 4.6 h contained 13% porosity, presumably due to decomposition. We also measured self-heating from exothermic decomposition reactions in three LX-17-1 samples.

## Acknowledgements

We thank LeRoy Green for many helpful discussions, and Paul Urtiew and Bruce Cunningham for their careful review of the manuscript. We also thank the Lawrence Livermore National Laboratory Surety Program for supporting this work, which was performed under the auspices of the US Department of Energy by Lawrence Livermore National Laboratory under contract no. W-7405-ENG-48.

## References

[1] J.R. Kolb, H.F. Rizzo, Propellants Explosives 4 (1979) 10.
[2] T.W. Stull, R.W. Ashcroft, Coefficient of Thermal Expansion of LX-17-1, Report No. MHSMP-89-13, Mason & Hanger, Silas Mason Co., Pantex Plant, Amarillo, TX, 1989.
[3] B. Dobratz, P.C. Crawford, LLNL Explosives Handbook, Report No. UCRL-52997 Change 2, Lawrence Livermore National Laboratory, Livermore, CA, 31 January 1985.
[4] J.C. Dallman, J. Wackerle, Temperature-dependent shock initiation of TATB-based high explosives, in: Proceedings of the 10th International Detonation Symposium, Report No. NSWCDD/MP-92/456, Naval Surface Warfare Center, White Oak, MD, 1993, p. 322.
[5] H.S. Carslaw, J.C. Jaeger, Conduction of Heat in Solids, Clarendon Press, Oxford, 1959.
[6] R.G. Garza, A Thermogravimetric Study of TATB and Two TATB-Based Explosives, Report No. UCRL-82723, Lawrence Livermore National Laboratory, Livermore, CA, 9 November 1979.
[7] J.R. Kolb, R.G. Garza, The Sublimation of 1,3,5-Triamino-2,4,6-trinitrobenzene (TATB), UCRL-85971, Lawrence Livermore National Laboratory, Livermore, CA, 20 October 1981.
[8] D.M. Hoffman, L.E. Caley, Polymer Eng. Sci. 26 (1986) 1489.
[9] W.E. Cady, L.E. Caley, Properties of Kel-F 800 Polymer, Report No. UCRL-52301, Lawrence Livermore National Laboratory, Livermore, CA, 21 July 1977.
[10] D.M. Hoffman, L.E. Caley, Organic coatings and plastics chemistry, in: Proceedings of the 181st National Meeting Presented at the American Chemical Society, 29 March–3 April 1981, Vol. 44, American Chemical Society, Atlanta, GA, p. 680.

[11] H.F. Rizzo, J.R. Humphrey, J.R. Kolb, Growth of 1,3,5-Triamino-2,4,6-trinitrobenzene (TATB) II. Control of Growth by Use of High Tg Polymeric Binders, Report No. UCRL-811889, Part II, Lawrence Livermore National Laboratory, Livermore, CA, 8 January 1980.

[12] R.R. McGuire, C.M. Tarver, Chemical decomposition models for the thermal explosion of confined HMX, TATB, RDX, and TNT explosives, in: Proceedings of 7th International Detonation Symposium, Report No. NSWC MP-82/334, Naval Surface Warfare Center, White Oak, MD, 1981, p. 56.